

The role of the Earth's mantle in controlling the frequency of geomagnetic reversals

Gary A. Glatzmaier^{*†}, Robert S. Coe^{*}, Lionel Hongre^{*} & Paul H. Roberts[‡]

^{*} Earth Sciences Department, University of California, Santa Cruz, California 95064, USA

[†] Institute of Geophysics and Planetary Physics, Los Alamos National Laboratory, Los Alamos, New Mexico 87545, USA

[‡] Institute of Geophysics and Planetary Physics, University of California, Los Angeles, California 90095, USA

A series of computer simulations of the Earth's dynamo illustrates how the thermal structure of the lowermost mantle might affect convection and magnetic-field generation in the fluid core. Eight different patterns of heat flux from the core to the mantle are imposed over the core–mantle boundary. Spontaneous magnetic dipole reversals and excursions occur in seven of these cases, although sometimes the field only reverses in the outer part of the core, and then quickly reverses back. The results suggest correlations among the frequency of reversals, the duration over which the reversals occur, the magnetic-field intensity and the secular variation. The case with uniform heat flux at the core–mantle boundary appears most 'Earth-like'. This result suggests that variations in heat flux at the core–mantle boundary of the Earth are smaller than previously thought, possibly because seismic velocity anomalies in the lowermost mantle might have more of a compositional rather than thermal origin, or because of enhanced heat flux in the mantle's zones of ultra-low seismic velocity.

The palaeomagnetic record of the Earth's magnetic field shows that the dipolar part, which is the dominant structure of the geomagnetic field outside the core, has reversed its polarity several hundred times during the past 160 million years (ref. 1). The reversal durations are relatively short (typically 1,000–6,000 years), compared with the constant polarity intervals between reversals. The intensity of the field decreases significantly during reversals. As global records of the palaeomagnetic field are not available, virtual geomagnetic poles (VGPs) have traditionally been computed from local measurements of the field direction using the equations for a purely dipolar field. Geomagnetic excursions (when VGPs deviate more than 45° in latitude from the geographic poles but do not reverse) tend to occur more frequently than full reversals. For example, there is evidence that as many as 14 excursions may have occurred since the last geomagnetic reversal 780,000 years ago².

Unlike the nearly constant periods of the solar magnetic cycle, geomagnetic polarity intervals vary from a few tens of thousands of years to superchrons, which have lasted tens of millions of years (ref. 1). The average duration of geomagnetic polarity intervals during the past 15 million years is about 200,000 years. The duration of a superchron, however, is roughly the timescale required for significant changes in the thermal structure of the Earth's mantle to take place as a result of subduction of tectonic plates and mantle convection. This observation and some noted correlations between plate tectonics, geomagnetic field intensity and reversal frequency have led to speculations that structural changes in the mantle may be influencing convection and magnetic-field generation in the fluid outer core^{3,4} (the geodynamo). In particular, it has been suggested that changes in both the total heat flow^{5–9} and the pattern of heat flux over the core–mantle boundary (CMB)^{3,5,8,10–15} may affect the geodynamo.

Several laboratory and numerical experiments have been conducted to study the effects of non-uniform thermal boundary conditions on non-magnetic convection^{16–19} and on magnetic convection^{20,21}. Here we present three-dimensional numerical simulations of the geodynamo, designed to study the effects of a non-uniform pattern of heat flux over the CMB.

Model description

Our results were obtained using the Glatzmaier–Roberts geodynamo model^{8,22}. This model produced the first dynamically

self-consistent computer simulation of the geodynamo²³: the three-dimensional, time-dependent thermodynamic, velocity and magnetic fields are solved simultaneously, each constantly feeding back to the others. The simulated magnetic field has a dipole-dominated structure and a spatially and time-dependent westward drift of the non-dipolar structure, both similar to the Earth's. A spontaneous magnetic dipole reversal also occurred in the original simulation²⁴. The latest version of this model employs more geophysically realistic heat-flux and magnetic-field boundary conditions, density stratification, inertia, and both thermal and compositional buoyancy sources²⁵.

To simulate hundreds of thousands of years with an average numerical time step (limited by the numerical solution method) of about 15 days, we can afford only a modest spatial resolution in our three-dimensional spherical-core model. That is, we use all spherical harmonics up to degree and order 21, and Chebyshev polynomials in radius up to degree 48 in the fluid outer core and up to 32 in the solid inner core. Consequently, the effects of the small unresolved turbulent eddies, which certainly exist in the Earth's low-viscosity fluid core, need to be represented by "eddy diffusion" in our model, as they are in models of the Earth's atmosphere and oceans and in other models of the geodynamo^{21,26–29}.

We have compared the solutions here with test simulations that have much greater spatial resolutions (one up to spherical harmonic degree 95 and another up to degree 239) and correspondingly less eddy diffusion. Although we see similar axisymmetric structures, the non-axisymmetric parts of the high-resolution solutions are (not unexpectedly) dominated by smaller-scale features. These resolved small-scale eddies provide additional induction of the large-scale magnetic field and so help maintain a more intense field. For example, the magnetic dipole moments for the results reported here tend to be lower than today's geomagnetic dipole moment (7.8×10^{22} A m²) and some are lower than the lowest estimate of its average value (4×10^{22} A m² over the past 160 million years)³⁰. Our high-resolution tests, on the other hand, produce field intensities that are similar to those of the Earth or greater.

In previous dynamo simulations we have, for simplicity, specified a heat flux from the core to the mantle that is uniform over the CMB. However, seismic tomography of the Earth's mantle³¹ and computer simulations of mantle convection³² suggest that the

temperature in the lower mantle can vary by hundreds of degrees Kelvin over lateral distances of roughly 1,000 kilometres. Convection in the fluid core just below the CMB is much more efficient because of the much smaller viscosity; lateral temperature variations there do not exceed 0.001 K. Consequently, large variations in the radial temperature gradient may occur over the CMB, and large

variations may thus also occur in the conduction of heat from the core to the mantle. This would result in slightly cooler (heavier) core fluid, on average, below the cold mantle and slightly warmer (lighter) fluid below the hot mantle, which modifies buoyancy and pressure-gradient forces throughout the fluid core. These forces, together with Coriolis forces (due to the component of the

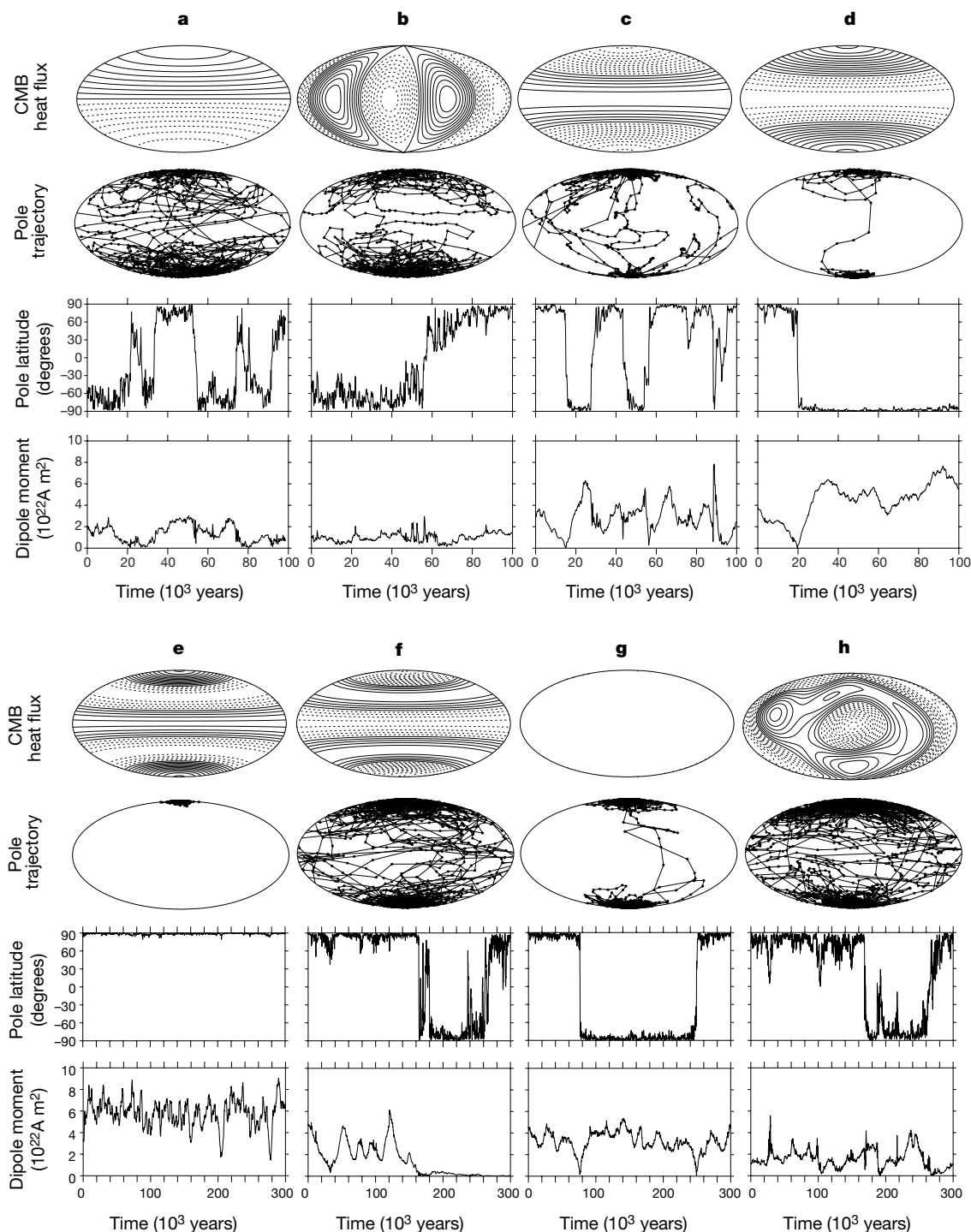


Figure 1 Dynamo simulations. The eight simulations have different imposed patterns of radial heat flux at the core–mantle boundary (CMB). Top row: the pattern of CMB heat flux in Hammer projections over the CMB with the geographical north pole at the top–centre and the south pole at the bottom–centre of each projection. Solid contours represent greater heat flux out of the core relative to the mean; broken contours represent less heat flux. The patterns are proportional to spherical harmonic of degree 1 and order 0 (pattern **a**), of degree 2 and order 2 (pattern **b**), of degree 2 and order 0 (patterns **c** and **d**) and of degree 4 and order 0 (patterns **e** and **f**). The uniform CMB heat-flux case is **g** and the

tomographic case is **h**. Second row: the trajectory of the south magnetic pole of the dipolar part of the magnetic field (observed outside the core) spanning the times indicated in the plots below; the marker dots are about 100 years apart. Third row: plots of the south magnetic pole latitude versus time. Fourth row: plots of the magnitude of the dipole moment versus time. **a–d** span 100,000 years; **e–h** span 300,000 years; the tick marks on the time axes are at intervals of 20,000 years (one dipole magnetic diffusion time). These simulations began long before the 0 times plotted here.

fluid flow perpendicular to the Earth's rotation vector) and Lorentz forces (due to the component of the electric current perpendicular to the magnetic field), drive complicated time-dependent circulations, providing a convective heat flux within the core that accommodates the imposed non-uniform conductive heat flux out of the core at the CMB.

To investigate the possible effects of the mantle's thermal structure on convection and magnetic-field generation in the fluid core, we compare eight dynamo simulations with different, time-independent, patterns of radial heat flux imposed at the CMB of the model. In each case, the total heat flow out of the core is maintained at 7.2×10^{12} W (7.2 TW), only 2.2 TW of which is due to the mean superadiabatic temperature gradient. One of the cases has uniform radial heat flux over the CMB (ref. 22). For the seven non-uniform cases we fix the peak variation of the heat flux (± 0.0446 W m⁻²) at the CMB, relative to the mean, at a value three times greater than the mean superadiabatic heat flux at the CMB; this is based on conservative estimates from mantle convection simulations³². Other than the non-uniform heat-flux boundary condition at the CMB, the model specifications for these simulations are identical to those of the uniform CMB heat-flux case, which was used as an initial condition for the non-uniform cases. In particular, all these cases have the Earth's rotation period and its magnetic dipole diffusion time of 20,000 years.

Results observed at the surface

The eight different CMB heat flux patterns are illustrated in the top row of Fig. 1. Those shown in Fig. 1a–f are simple patterns chosen for this sensitivity study. The uniform CMB heat-flux case (case g) is illustrated in Fig. 1g. The 'tomographic' case (case h), shown in Fig. 1h, is based on the seismic tomography of the lowermost mantle for today's Earth^{8,31} (up to spherical harmonic degree and order four). Cases a–d (Fig. 1a–d) were each run for at least 100,000 years; cases e–h (Fig. 1e–h) were run for at least 300,000 years (15 magnetic dipole diffusion times).

The CMB heat flux in case a is forced to be axisymmetric but highly antisymmetric with respect to the equator; the maximum heat flux out of the core occurs at the geographical north pole and the minimum at the south pole. As observed from outside the core, the direction of the magnetic dipole moment is highly variable, reversing its polarity several times during the 100,000 years displayed in Fig. 1a. The magnitude of the magnetic dipole moment, which includes both the axial and equatorial components, is lower than in several of the other cases and is close to zero during the reversals.

The sensitivity of a longitudinally varying CMB heat flux is tested in case b of Fig. 1; it also varies in latitude but is symmetric with respect to the equator. As in case a, the amplitude of the dipole moment is low, but, unlike case a, only one dipole reversal occurs during the 100,000 years. As seen in Fig. 1b, the pole reversal path seems to follow a longitude band of high CMB heat flux (cold mantle) until reaching the equatorial region where it jumps to the other 'preferred' longitude band, in accord with some palaeomagnetic reversal analyses^{13,33,34} (based on VGPs). However, here, with only one reversal, it could easily be a coincidence. Indeed, some other analyses of palaeomagnetic reversal records suggest that there is no actual longitudinal bias in the distribution of transitional field VGPs (refs 35–37).

The sensitivity of a latitudinally varying CMB heat flux that is axisymmetric and symmetric about the equator is tested in cases c–f. The imposed patterns of CMB heat flux (relative to the mean) are opposite in cases c and d. In both cases, the amplitude of the dipole moment decreases significantly during reversals, but case c reverses more frequently than does case d.

Cases e and f test the effects of greater latitudinal structure in the CMB heat-flux pattern. As seen in Fig. 1, the imposed CMB heat flux for case e peaks at the geographical poles and at the equator and

reaches its minimum at mid-latitude. This is our most efficient case; that is, the amplitude of the dipole moment is, on average, larger than for the other cases. Although the amplitude does have considerable variation, the direction of the dipole moment is always closely aligned with the axis of rotation; no reversal or excursion occurs during the 300,000 years.

Case f, with the opposite pattern of imposed CMB heat flux (relative to the mean), has significantly greater secular variation of the field and a smaller average dipole moment. It reverses after about 160,000 years, but the amplitude of the dipole moment does not recover during the 140,000 years after this first reversal. Before the reversal the magnetic energy integrated throughout the outer core is at least 1,000 times greater than the integrated kinetic energy of the fluid flow (relative to the rotating frame of reference). After this first reversal the magnetic energy is, on average, only about ten times the kinetic energy; it decreases by almost another factor of ten during the second reversal and remains at this level. This is similar to recent results from a number of other dynamo simulations³⁸. Magnetic dipole reversals did not occur in those simulations, but, in order to test the solutions, the magnetic field intensities were manually reduced by a factor of 20 or more during the simulations (within one numerical time step). In a few of the cases the intensities, instead of recovering, remained at roughly the level to which they were artificially reduced. Possibly (as may also apply to case f) the dynamo solutions for those parameters (and, in case f, the CMB conditions) were very close to those for neutral growth of the field. It is also plausible that Venus and/or Mars may have lost strong global magnetic fields in this way.

Our non-uniform CMB heat-flux cases were started from the uniform CMB heat-flux case (Fig. 1g), which was started from our original simulation²³. Case g ran for 500,000 years (25 magnetic dipole diffusion times, 15 million numerical time steps), only 300,000 years of which are displayed. The reversal record for this case is similar to that of the Earth: the axisymmetric part of the field is very stable and dipole-dominated for 230,000 years, then the dipole quickly reverses in ~1,000 years (it takes ~4,000 years for the axial dipole to become dominant again), is stable for the next 170,000 years, then quickly reverses a second time, and is relatively stable for the remaining 100,000 years. This case also shows, more clearly than most of the others, a significant decrease in the dipole moment during reversals (Fig. 1g), as seen in the palaeomagnetic record. A smaller decrease accompanies an excursion that occurs after the time interval displayed in Fig. 1g.

The tomographic case (Fig. 1h), which has an imposed CMB heat flux patterned after today's Earth³¹ (higher heat flux on the 'ring around the Pacific' of high seismic velocity), was chosen to test a possibly more geophysically realistic simulation. We have previously described the first 100,000 years of this case (ref. 8), before the first reversal occurred. The duration of the first reversal is about 6,000 years, whereas the second reversal lasts more than 20,000 years, depending on how the beginning and end of this transition is defined. In addition, several aborted reversals or excursions take place during the simulation. The dipole path of the first reversal strongly overlaps the 'preferred' longitude band of high CMB heat flux that lies underneath the Americas (on the right side of Fig. 1h). Likewise, the density of transitional VGPs from observation points distributed evenly all over the globe also peaks there. The dipole path of the second reversal is much more complex than for the first, sampling many longitudes. So is the density of the transitional VGPs, which has a pronounced low corresponding to the CMB heat-flux low under the Pacific basin and a broad high that extends eastward from 270° E to 135° E, with small peaks centred at 300° E and 35° E. These results and those mentioned above for case b suggest that longitudinally varying CMB heat flux may geographically bias reversal transition paths, but obviously a much longer simulation, with many more reversals than two, would be needed to assess the statistical significance of such correlations. For example,

the two dipole reversal paths of case g, which has no imposed CMB heat-flux bias, just happen to occur in the same longitude band. A more detailed presentation of the characteristics of these reversals will be published elsewhere.

In addition to comparing the frequencies of reversals, we can compare the general structures of the surface fields for the different cases to that of the Earth's. The geomagnetic field at the Earth's surface is traditionally described in terms of gauss coefficients, g_l^m and h_l^m , where l and m are, respectively, the degree and order in the spherical harmonic expansion of the surface field¹. Over the past 5 Myr the Earth's axial quadrupole field, g_2^0 , has had, on average, the same sign as the axial dipole field, g_1^0 , and about 0.04 of its magnitude^{39–43}.

Other than during reversals and excursions, the axial dipole also strongly dominates in our simulations, but the sign relationship between the three main modes is case-dependent. For case a, the axial quadrupole and the axial octupole, g_3^0 , usually have the same sign and reverse together; this reflects the greater field intensity in the northern hemisphere where the heat flux is greater. The dipole and octupole reverse roughly together in cases c and d, maintaining opposite signs in case c and same signs in case d; this reflects the greater field intensity (relative to a pure dipole) maintained in the equatorial region for case c and in the polar regions for case d. In case b, the axial dipole and quadrupole usually have the same sign, opposite the axial octupole, and they all reverse at about the same time. The three modes also reverse approximately together in case g, but the axial quadrupole and octupole nearly always have the same sign, opposite to the sign of the axial dipole. No clear sign relationships persist in cases e, f, h or in our high-resolution versions of case g.

The surface field in our most stable case, e, is strongly dominated by the axial dipole, more so than the Earth's, with the magnitudes of g_2^0 and g_3^0 being on average 0.01 and 0.02 of the magnitude of g_1^0 , respectively. Case f, which has the opposite CMB heat-flux pattern, is our least stable case in terms of maintaining a strong magnetic field. For this case, f, the magnitudes of g_2^0 and g_3^0 are on average 0.05 and 0.04 of g_1^0 before the first dipole reversal. After this reversal, g_1^0 is on average 20 times smaller than it was before; the relative decreases in g_2^0 and g_3^0 are less.

For the other cases, especially c, d and g, which have strong dipolar dominance when not reversing, we see a correlation between the dipolar (W_D) and non-dipolar (W_{ND}) magnetic energy densities (averaged over the surface) during reversals that agrees quite well with the early heuristic model of Cox⁴⁴. Our reversals usually occur when a significant decrease in W_D coincides with an increase in W_{ND} .

Finally, we compare the variability of the surface field to that of the Earth's. Whereas the pole latitude (Fig. 1) provides a measure of the variability of the magnetic dipole, the dispersion of the VGP provides a measure of the directional variability of the entire field at the surface. First the angular standard deviation of the VGPs (from the geographical pole, which is essentially the same as the average magnetic pole) is calculated at over 2,500 sites distributed over the globe, roughly every 100 years, following the usual palaeomagnetic practice of cutting out VGPs that are further than 45° from the geographical poles to exclude reversals and excursions¹. Averaging these in longitude and combining the northern and southern hemispheres provides a VGP dispersion as a function of latitude. An estimate of the Earth's VGP dispersion (ref. 1) over the last 5 Myr (obviously based on much less spatial and temporal resolution than we enjoy) is about 13° at the equator, increasing to about 20° at 65 degrees latitude.

For case a the VGP dispersion is 26° at the equator and decreases slightly with latitude, whereas case b increases from 22° at the equator to 26° poleward. The VGP dispersion for case c is more like the Earth's: 16° at the equator, increasing to 22° at high latitude. Case e is directionally very stable, as the small deviations of its magnetic pole from the geographical pole (Fig. 1e) also suggest; its VGP

dispersion is only 3° at the equator, increasing to about 8° poleward. Very little latitudinal variation is seen in the VGP dispersions for cases d, f, g and h; case d decreases slightly from 10°, case f increases slightly from 14°, case g increases slightly from 11°, and case h increases slightly from 22°. Our higher-resolution version of case g, which has many more degrees of freedom (up to spherical harmonic degree 95), has a VGP dispersion that increases with latitude (8° at the equator, 25° at high latitude), more like the Earth's. However, this is mainly a spatial average because the simulation at this resolution is relatively short.

Dynamics inside the core

The intensity and directional measurements of the field observed above the core are subtle manifestations of the much more intense and complicated field inside the core^{23,24}. We consider, for example, the first reversal of case h. 'Snapshots' of the radial component of the field at the CMB and at what would be the surface of the Earth are displayed in Fig. 2 at roughly 3,000-year intervals, spanning the reversal. The plots for a given snapshot illustrate how the larger-scale structures, such as the dipole, decrease less rapidly with radius, resulting in a much smoother and more large-scale-dominated field at the surface. Corresponding snapshots of the longitudinally averaged field through the interior are also shown. The reversal of the dipolar part of the field begins near the CMB and progresses inward until finally, about 3,000 years after the poloidal field has reversed at the surface (Fig. 2c), the poloidal and toroidal parts of the field reverse (Fig. 2d) inside the 'tangent cylinder', an imaginary cylinder tangent to the solid inner-core equator. Opposite magnetic polarities can exist inside and outside the tangent cylinder²², as seen in Fig. 2c, because the dynamics in these two regions differ significantly. For example, Coriolis forces are always perpendicular to the axis of rotation, whereas buoyancy forces are mostly parallel to the axis inside the tangent cylinder and perpendicular to the axis outside the cylinder; this basic difference in the balance of forces is one of the factors that makes this problem so interesting.

The sequence in Fig. 2 is the opposite of what occurred in our first simulated reversal²⁴. In that reversal the toroidal field reversed first, then the poloidal field inside the tangent cylinder reversed, and finally the poloidal field outside the tangent cylinder reversed. The reversal recently seen in a two-and-a-half-dimensional simulation⁹ (one for which there is insufficient resolution in the third dimension) began at the inner-core boundary. However, for most of the reversals in Fig. 1, the field first reverses outside the tangent cylinder and later inside it. Even the two reversals in case g, with the uniform CMB heat flux, begin outside the tangent cylinder. They both last about 4,000 years when observed at the surface. This includes the time needed to recover dipole dominance; the duration of a reversal at the surface is based on qualitative judgements of its beginning and end times. In addition, a full reversal is not complete until the field inside the tangent cylinder also reverses. For the first reversal of case g, this takes roughly another 2,000 years; the second reversal takes longer, another 9,000 years. The three-dimensional time-dependent details of each reversal presented here differ significantly, as they are likely to do for every geomagnetic reversal that has occurred.

The structure and evolution of the magnetic field is determined by how and where it is twisted and sheared by the fluid flow, which itself is influenced by magnetic (Lorentz) forces. The flow is also greatly influenced by the planetary rotation, the geometry of the inner and outer cores, and the imposed pattern of CMB heat flux. In addition, the flow is driven by thermal and compositional buoyancy sources, which in turn are advected by the flow. This complicated nonlinear system of feedbacks provides an abundant variety of possible solutions that do not lend themselves to simple linear explanations. In general, magnetohydrodynamic instabilities are always occurring, but they usually die away. Once in many attempts, though, an instability continues to grow while the original field polarity decays and the new polarity takes over.

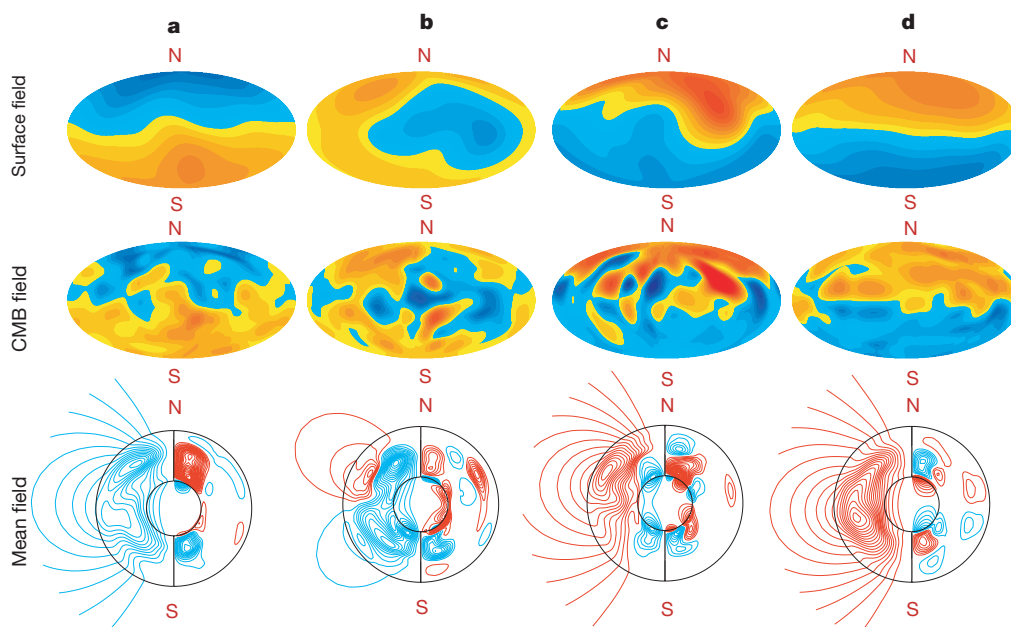


Figure 2 Progression of the magnetic field. A sequence of snapshots is shown of the longitudinally averaged magnetic field through the interior of the core (bottom row), of the radial component of the field at the core–mantle boundary, CMB (middle row), and at what would be the surface of the Earth (top row) displayed at roughly 3,000-year intervals, spanning the first dipole reversal of case h in Fig. 1. In the bottom row of plots, the small circle represents the inner core boundary and the large circle represents the CMB. The poloidal field is shown as magnetic field lines on the left-hand sides of these plots (blue lines are clockwise and red lines are anticlockwise). The toroidal field direction and

intensity are represented as contours (not magnetic field lines) on the right-hand sides (red lines are eastward and blue lines are westward). In the middle and top rows, Hammer projections of the entire CMB and the surface are used to display the radial field (the two different surfaces are displayed as the same size). Yellow shades represent the outward-directed field and blue shades represent the inward-directed field; the surface field, which is typically an order of magnitude weaker, was multiplied by 10 to enhance the colour contrast.

The highly unstable and inefficient magnetic-field generation of case a occurs because the equatorially antisymmetric thermal condition imposed at the CMB is not preferred by the natural dynamics of a rapidly rotating convecting fluid, which attempts to maintain a high degree of thermal symmetry with respect to the equator. Instead, by forcing greater heat flux out of the northern hemisphere, that hemisphere tends to be cooler than the southern hemisphere. This drives hemispheric oscillations in the flow and field amplitudes with a period of ~1,000 years; these oscillations usually lead to a magnetic reversal. However, the reversals seen from outside the core between elapsed model times 20,000 years and 30,000 years (Fig. 1a, third row) actually only occur outside the tangent cylinder. That is, the original polarity of the poloidal and toroidal parts of the field inside the tangent cylinder does not reverse until about time 35,000 years in Fig. 1a when a full magnetic reversal occurs throughout the core. It is likely that cryptochrons (a pair of reversals usually less than 10,000 years apart) and some excursions seen in the palaeomagnetic record² have also occurred only outside the tangent cylinder (S. P. Lund, personal communication).

The relatively large secular variations of the field in cases b and h are due to the longitudinal variations of their CMB heat fluxes²⁰. Convection outside the tangent cylinder, which is mainly in the form of high-wavenumber columnar cells, is continually perturbed by the low-wavenumber thermal boundary condition as the convective pattern propagates westward relative to the mantle⁸. The resulting disturbances in the fluid flow, especially near the CMB, generate disturbances in the magnetic field.

The greater magnetic stability of case d relative to case c and of case e relative to case f indicates a preference for outward convective heat flux in the polar regions, provided by the warm outward-directed part of the thermal wind there⁸. Notice also that the duration of the reversal in case d (Fig. 1) is shorter than those of case c and certainly case f. That is, forcing greater heat flux through the CMB in the polar regions appears to be more compatible with the rotating magnetic convection below the CMB and reinforces the

shear flow on the tangent cylinder, which generates a dipolar field closely aligned with the axis of rotation.

Discussion

The number of reversals that occur in our simulations is far too few for statistical analysis and, in addition, the model should be run with lower viscosity and higher resolution (as computer technology improves), but we can nevertheless make a few observations here. The only simulation that has not yet produced a dipole reversal is case e. Its VGP dispersion is the lowest, and its average dipole moment and dipole dominance are the greatest. Cases d and g also have relatively small VGP dispersions and large average dipole moments; they also have relatively low reversal frequencies and the shortest reversal durations (in terms of pole latitude). The limitations of the short simulation times are apparent in case b, which has a relatively large VGP dispersion but has reversed only once in 100,000 years. However, cases a and c have the highest reversal frequencies and relatively large VGP dispersions.

Correlations like these have been found in the palaeomagnetic record^{1,14,30,44–47}, although there too, exceptions exist⁴⁷. The correlation between high dipole reversal frequency and low dipole moment has also been seen in two-dimensional kinematic dynamo model calculations⁴⁸. Our three-dimensional simulations suggest that the geodynamo is more stable (it has small reversal frequency, secular variation and reversal durations) and more efficient (it has a large dipole moment) when the lateral pattern of diffusive heat flux from the core to the mantle matches the natural time-averaged pattern of convective heat flux deep within the fluid core. This occurs (in our simulations) when the CMB heat flux is axisymmetric and equatorially symmetric, with maxima in the polar regions. These results suggest that superchrons of constant dipole polarity may have occurred under similar conditions and that the pattern of CMB heat flux needs to change significantly to produce a measurable change in reversal frequency.

But how large are the lateral variations in the Earth's CMB heat

flux? Comparing the uniform CMB heat flux case, g, and the tomographic case, h, may be helpful. Although both (so far) have reversal frequencies similar to the Earth's, the excursion frequency may be too high for h and too low for g. However, the VGP dispersion for g, especially the high-resolution version, is more like the Earth's than that for h, and the duration of the second reversal of h is much longer than the more Earth-like ones of g. These preliminary results suggest that the large lateral variations we imposed on the CMB heat flux for case h (inferred from simulations of mantle convection and from large-scale seismic tomography of the lowermost mantle) may be much larger than the Earth's core in fact experiences. If this were the case, our results support two plausible hypotheses (or a combination of them) that have been discussed previously. The seismic velocity anomalies measured in the lowermost mantle may be more a compositional effect than a thermal effect. Or, the CMB heat flux below warm mantle (slow seismic velocity, where we assumed minimum heat flux) may be enhanced by greater mantle thermal conductivity (due to iron enrichment) and possibly by small-scale convection of partial melt corresponding to the ultra-low seismic velocity zones^{49,50} measured in these regions. □

Received 16 June; accepted 10 September 1999.

1. Merrill, R. T., McElhinny, M. W. & McFadden, P. L. *The Magnetic Field of the Earth: Paleomagnetism, the Core, and the Deep Mantle* (Academic, San Diego, 1996).
2. Lund, S. P. *et al.* Geomagnetic field excursions occurred often during the last million years. *Eos* **79**, 178–179 (1998).
3. Cox, A. & Doell, R. R. Long period variations of the geomagnetic field. *Bull. Seismol. Soc. Am.* **54**, 2243–2270 (1964).
4. Vogt, P. R. Changes in geomagnetic reversal frequency at times of tectonic change: evidence for coupling between core and upper mantle processes. *Earth Planet. Sci. Lett.* **25**, 313–321 (1975).
5. Jones, G. M. Thermal interaction of the core and the mantle and long-term behavior of the geomagnetic field. *J. Geophys. Res.* **82**, 1703–1709 (1977).
6. Loper, D. E. & McCartney, K. Mantle plumes and the periodicity of magnetic field reversals. *Geophys. Res. Lett.* **82**, 1703–1709 (1977).
7. McFadden, P. L. & Merrill, R. T. Lower mantle convection and geomagnetism. *J. Geophys. Res.* **89**, 3354–3362 (1984).
8. Glatzmaier, G. A. & Roberts, P. H. Simulating the geodynamo. *Contemp. Phys.* **38**, 269–288 (1997).
9. Sarson, G. R. & Jones, C. A. A convection driven geodynamo reversal model. *Phys. Earth Planet. Inter.* **111**, 3–20 (1999).
10. Hide, R. On the Earth's core-mantle interface. *Q. J. R. Meteorol. Soc.* **96**, 579–590 (1970).
11. Goodacre, A. K. An intriguing empirical correlation between the Earth's magnetic field and plate motions. *Phys. Earth Planet. Inter.* **49**, 3–5 (1987).
12. Bloxham, J. & Gubbins, D. Thermal core-mantle interactions. *Nature* **325**, 511–513 (1987).
13. Laj, C., Mazaud, A., Weeks, R., Fuller, M. & Herrero-Bervera, E. Geomagnetic reversal paths. *Nature* **351**, 447 (1991).
14. McFadden, P. L. & Merrill, R. T. Fundamental transitions in the geodynamo as suggested by paleomagnetic data. *Phys. Earth Planet. Inter.* **91**, 253–260 (1995).
15. Gallet, Y. & Hulot, G. Stationary and nonstationary behavior within the geomagnetic polarity timescale. *Geophys. Res. Lett.* **24**, 1875–1878 (1997).
16. Hart, J. E., Glatzmaier, G. A. & Toomre, J. Space-laboratory and numerical simulations of thermal convection in a rotating hemispherical shell with radial gravity. *J. Fluid Mech.* **173**, 519–544 (1986).
17. Bolton, E. W. & Saylor, B. S. The influence of lateral variations of thermal boundary conditions on core convection: Numerical and laboratory experiments. *Geophys. Astrophys. Fluid Dyn.* **60**, 369–370 (1991).
18. Zhang, K. & Gubbins, D. On convection in the earth's core driven by lateral temperature variations in the lower mantle. *Geophys. J. Int.* **108**, 247–255 (1992).
19. Sun, Z.-P., Schubert, G. & Glatzmaier, G. A. Numerical simulations of thermal convection in a rapidly rotating spherical shell cooled inhomogeneously from above. *Geophys. Astrophys. Fluid Dyn.* **75**, 199–226 (1994).
20. Olson, P. & Glatzmaier, G. A. Magnetoconvection and thermal coupling of the Earth's core and mantle. *Phil. Trans. R. Soc. Lond. A* **354**, 1413–1424 (1996).
21. Sarson, G. R., Jones, C. A. & Longbottom, A. W. The influence of boundary region heterogeneities on the geodynamo. *Phys. Earth Planet. Inter.* **101**, 13–32 (1997).
22. Glatzmaier, G. A. & Roberts, P. H. An anelastic evolutionary geodynamo simulation driven by compositional and thermal convection. *Physica D* **97**, 81–94 (1996).
23. Glatzmaier, G. A. & Roberts, P. H. A three-dimensional convective dynamo solution with rotating and finitely conducting inner core and mantle. *Phys. Earth Planet. Inter.* **91**, 63–75 (1995).
24. Glatzmaier, G. A. & Roberts, P. H. A three-dimensional self-consistent computer simulation of a geomagnetic field reversal. *Nature* **377**, 203–209 (1995).
25. Braginsky, S. I. & Roberts, P. H. Equations governing convection in Earth's core and the geodynamo. *Geophys. Astrophys. Fluid Dyn.* **79**, 1–97 (1995).
26. Kuang, W. & Bloxham, J. An Earth-like numerical dynamo model. *Nature* **389**, 371–374 (1997).
27. Christensen, U., Olson, P. & Glatzmaier, G. A. A dynamo model interpretation of geomagnetic field structures. *Geophys. Res. Lett.* **25**, 1565–1568 (1998).
28. Busse, F. H., Grote, E. & Tilgner, A. On convection driven dynamos in rotating spherical shells. *Studia Geophys. Geodyn.* **42**, 1–6 (1998).
29. Sakuraba, A. & Kono, M. Effect of the inner core on the numerical solution of the magneto-hydrodynamic dynamo. *Phys. Earth Planet. Inter.* **111**, 105–121 (1999).
30. Juez, M. T., Tauxe, L., Gee, J. S. & Pick, T. The intensity of the Earth's magnetic field over the past 160 million years. *Nature* **394**, 878–881 (1998).
31. Su, W.-J., Woodward, R. L. & Dziewonski, A. N. Degree-12 model of shear velocity heterogeneity in the mantle. *J. Geophys. Res.* **99**, 6945–6980 (1994).
32. Tackley, P. J., Stevenson, D. J., Glatzmaier, G. A. & Schubert, G. Effects of multiple phase transitions in a 3-D spherical model of convection in the Earth's mantle. *J. Geophys. Res.* **99**, 15,877–15,901 (1994).
33. Clement, B. M. & Kent, D. V. A southern hemisphere record of the Matuyama-Brunhes polarity reversal. *Geophys. Res. Lett.* **18**, 81–84 (1991).
34. Hoffman, K. A. Dipolar reversal states of the geomagnetic field and core-mantle dynamics. *Nature* **359**, 789–794 (1992).
35. McFadden, P. L., Barton, C. E. & Merrill, R. T. Do virtual geomagnetic poles follow preferred paths during geomagnetic reversals? *Nature* **361**, 342–344 (1993).
36. Prevot, M. & Camps, P. Absence of preferred longitude sectors for poles from volcanic records of geomagnetic reversals. *Nature* **366**, 53–57 (1993).
37. Quidelleur, X. & Valet, J.-P. Paleomagnetic records of excursions and reversals: Possible biases caused by magnetization artefacts. *Phys. Earth Planet. Inter.* **82**, 27–48 (1994).
38. Christensen, U., Olson, P. & Glatzmaier, G. A. Numerical modeling of the geodynamo: A systematic parameter study. *Geophys. J. Int.* **138**, 393–409 (1999).
39. Cox, A. The frequency of geomagnetic reversals and the symmetry of the non-dipole field. *Rev. Geophys. Space Phys.* **13**, 35–51 (1975).
40. Merrill, R. T. & McElhinny, M. W. Anomalies in the time averaged magnetic field and their implications for the lower mantle. *Rev. Geophys. Space Phys.* **15**, 309–323 (1977).
41. Quidelleur, X., Valet, J.-P., Courtillot, V. & Hulot, G. Long-term geometry of the geomagnetic field for the last 5 million years—an updated secular variation database. *Geophys. Res. Lett.* **21**, 1639–1642 (1994).
42. Johnson, C. & Constable, C. The time-averaged field as recorded by lava flows over the past 5 Myr. *Geophys. J. Int.* **122**, 489–519 (1995).
43. McElhinny, M. W., McFadden, P. L. & Merrill, R. T. The time-averaged field 0–5 Ma. *J. Geophys. Res.* **101**, 25007–25027 (1996).
44. Cox, A. Lengths of geomagnetic polarity intervals. *J. Geophys. Res.* **73**, 3249–3260 (1968).
45. Irving, E. & Pullaiah, G. Reversals of the geomagnetic field, magnetostratigraphy, and relative magnitude of secular variation in the Phanerozoic. *Earth Sci. Rev.* **12**, 35–64 (1976).
46. Pal, P. C. & Roberts, P. H. Long-term polarity stability and strength of the geomagnetic dipole. *Nature* **331**, 702–705 (1990).
47. Tauxe, L. & Hartl, P. 11 million years of Oligocene geomagnetic field behavior. *Geophys. J. Int.* **128**, 217–229 (1997).
48. Olson, P. & Hagee, V. L. Geomagnetic polarity reversals, transition field structure, and convection in the outer core. *J. Geophys. Res.* **95**, 4609–4620 (1990).
49. Garnero, E. J. & Helmberger, D. V. Seismic detection of a thin laterally varying boundary layer at the base of the mantle beneath the central-Pacific. *Geophys. Res. Lett.* **23**, 977–980 (1996).
50. Lay, T., Williams, Q. & Garnero, E. J. The core-mantle boundary layer and deep Earth dynamics. *Nature* **392**, 461–468 (1998).

Acknowledgements

We thank R. T. Merrill for suggesting this numerical study. This work was supported by the Institute of Geophysics and Planetary Physics, the Los Alamos LDRD program, the University of California Research Partnership Initiatives program, the NSF Geophysics program and the NASA HPCC/ESS Grand Challenge program. Computing resources were provided by the Los Alamos Advanced Computing Laboratory, the San Diego Supercomputing Center, the Pittsburgh Supercomputing Center, the National Center for Supercomputing Applications, the Texas Advanced Computing Center, the Goddard Space Flight Center, and the Marshall Space Flight Center.

Correspondence and requests for materials should be addressed to G.A.G. (e-mail: glatz@es.ucsc.edu).